

Simulation of a 1550 nm InGaAsP-InP transistor laser

Wei Shi^a, Zigang Duan^{b*}, Raha Vafaei^a, Nicolas Rouger^a, Behnam Faraji^a, Lukas Chrostowski^{a†}

^aDepartment of Electrical and Computer Engineering, University of British Columbia, Vancouver, BC V6T 1Z4, Canada.

^bKey Laboratory of Optoelectronic Devices and Systems of Ministry of Education and Guangdong Province, Shenzhen University, Shenzhen 518060, China.

ABSTRACT

A 1550 nm InGaAsP-InP multiple-quantum-well (MQW) transistor laser is numerically modeled. The proposed structure has a deep-ridge waveguide and asymmetric doping profile in the base (i.e. only the part below QWs of the base is doped) which provides good optical and electrical confinement and effectively reduces the lateral leakage current and optical absorption. The important physical models and parameters are discussed and validated by modeling a conventional ridge-waveguide laser diode and comparing the results with the experiment. The simulation results of the transistor laser demonstrate a low threshold (< 10 mA) and a $> 25\%$ slope efficiency with the current gain of $2 \sim 4$. The optical saturation and voltage-controlled operation are also demonstrated.

Keywords: Transistor laser, 1550 nm multiple quantum wells, InGaAsP

1. INTRODUCTION

As a functional integration of a transistor and a laser, the transistor laser can take an electrical input signal and simultaneously output an optical signal and an electrical signal which are coupled to each other.¹ It is very interesting not only for academic research but also for practical applications. For example, we can use the electrical output signal to monitor the optical output in order to achieve dynamic stabilization and feedback control without additional optical elements. The transistor laser also has a potential for high-speed applications due to its unique carrier dynamics which are different from either normal bipolar junction transistors (BJTs) or laser diodes.² The analytical modeling demonstrated the difference between common-base and common-emitter configurations and predicted a bandwidth enhancement for direct laser modulation in the common-base configuration.³ Another interesting feature is the voltage-controlled operation that is promising for optoelectronic integration.⁴ The voltage-controlled direct modulation of a tunnel junction transistor laser was presented recently.⁵

While the transistor laser has demonstrated many interesting features and great potential in applications, it has serious challenges. A heavily doped base is typically used in modern heterojunction bipolar transistors (HBTs) to reduce electrical resistance for high-speed consideration and was also used in the demonstrated transistor lasers^{1,6} where the potential of an enhanced small-signal modulation bandwidth was attributed to the reduced carrier lifetime due to the high doping density.⁷ However the analytical modeling including the quantum capture and escape processes showed that the transistor laser's small-signal modulation performance in the common-emitter configuration is similar to the conventional laser diodes with a separate confinement heterostructure (SCH),⁸ although we can have a higher bandwidth by sacrificing the gain of the AC response, e.g., by common-base configuration.^{2,3} Therefore high doping density in the base may not be desired since it is not necessary for higher bandwidth and can cause serious problems of excessive carrier recombination and optical absorption. To date, the demonstrated transistor lasers have relatively high threshold and low optical power.^{5,9} Continuous operation at $\sim 1.55 \mu\text{m}$ was only achieved at a very low temperature (-180°C).⁶

In this paper, a 1550 nm transistor laser structure based on InGaAsP-InP material system is proposed and numerically modeled by the 2D commercial laser simulator LASTIP.¹⁰ The laser has a deep-ridge waveguide structure and an asymmetric doping profile in the base (i.e., only the part below the QWs of the base is doped). The proposed device structure is demonstrated in Section 2. The physical models and key parameters are

* Email: zgduan@szu.edu.cn

† Email: lukasc@ece.ubc.ca

described in Section 3. A ridge-waveguide laser diode is simulated and compared with the experiment to evaluate the models and parameters. The simulation results are presented in Section 4. Section 5 is the conclusion.

2. DEVICE DESIGN

The epitaxial structure of the 1550 nm transistor laser is shown in Table 1. It is an InGaAsP/InP n-p-n HBT structure with the QWs (1.2% compressively strained InGaAsP) buried in the center of the InGaAsP (1.24 μm) waveguide region. Different from the previous transistor lasers, the top waveguide is undoped for reducing carrier recombination and optical absorption. The heavily p-doped layer for the p contact is placed away below the QWs for preventing dopant diffusion into the QWs which can significantly affect the optical gain.¹¹ The p contact on InGaAsP might be challenging. $\text{In}_{0.53}\text{Ga}_{0.47}\text{As}$ is widely used as the p contact layer in 1550 nm laser diodes although it has smaller band-gap than the QWs since it is usually far away from the active region. However we cannot use $\text{In}_{0.53}\text{Ga}_{0.47}\text{As}$ as the base contact because it will be much closer to the peak of the optical mode in the transistor laser than in normal laser diodes and hence can induce a strong optical loss. A p contact on InGaAsP has relatively higher resistance than on $\text{In}_{0.53}\text{Ga}_{0.47}\text{As}$ but can form good ohmic contact with a resistance as low as $\sim 10^{-6} \Omega\text{cm}^2$.^{12,13} Using InP as the collector can increase the breakdown voltage but may block the electrons and hence reduce the electrical gain ($\beta = \Delta I_C / \Delta I_B$, where I_C and I_B are collector and base currents, respectively). Our design uses a collector consisting of 3 layers: $\text{In}_{0.76}\text{Ga}_{0.24}\text{As}_{0.53}\text{P}_{0.47}$ (the same material as the base), InP, and a compositional grading layer between them. The reverse biased base-collector junction introduces a gradient in the carrier distribution in the waveguide/base which provides the electrical output (I_C) in addition to the optical output.

Table 1. The proposed epitaxial structure used in the numerical simulation for the 1550 nm transistor laser.

Layer	Composition	Thickness (nm)	Doping ($10^{18}/\text{cm}^3$)
Cladding, Emitter contact	InP	1800	n, 1.0 \sim 3.0
Top Waveguide	$\text{In}_{0.76}\text{Ga}_{0.24}\text{As}_{0.53}\text{P}_{0.47}$	100	Undoped
6 Wells / 5 Barriers	$\text{In}_{0.81}\text{Ga}_{0.19}\text{As}_{0.24}\text{P}_{0.76}$ / $\text{In}_{0.76}\text{Ga}_{0.24}\text{As}_{0.53}\text{P}_{0.47}$	6 / 9	Undoped
Bottom Waveguide	$\text{In}_{0.76}\text{Ga}_{0.24}\text{As}_{0.53}\text{P}_{0.47}$	40	Undoped
Base contact	$\text{In}_{0.76}\text{Ga}_{0.24}\text{As}_{0.53}\text{P}_{0.47}$	40	p+, 10
Collector	$\text{In}_{0.76}\text{Ga}_{0.24}\text{As}_{0.53}\text{P}_{0.47}$	20	Undoped
Grading	$\text{In}_{0.76}\text{Ga}_{0.24}\text{As}_{0.53}\text{P}_{0.47} \sim \text{InP}$	20	Undoped
Collector	InP	40	Undoped
Sub-collector	InP	1200	n, 1.0
Substrate, Collector contact	InP	-	n, 3.0

The laser is designed to be a 250 μm long edge-emitter with 90% and 30% reflectivities for the front and back facets, respectively. The ridge waveguide is 3 μm wide. The whole device has a symmetric layout with the emitter contact on the top of the ridge, the collector contact on the backside of the wafer, and two base contacts on the top of the two sides of the base contact layer. The wafer is to be etched through the QWs down to the heavily doped p-contact layer. The lateral leakage current is one of the main sources of the threshold in the ridge-waveguide lasers and is more harmful in the transistor lasers with heavily doped waveguide layer above the QWs due to the shorter carrier lifetime, hence in our design the region above the QWs is undoped. The deeply etched mesa provides better optical and electrical confinement and removes the necessity of the heavily doped layer above the QWs. Therefore it can effectively reduce the lateral leakage current and optical absorption. The disadvantage of this deep-ridge design is that it requires high etching accuracy since there is no etching-stop layer in the waveguide.

3. PHYSICAL MODELS AND KEY PARAMETERS

All the physical models are well established in the 2D simulator LASTIP . Here we discuss the aspects that are crucial to our study (e.g., carrier recombination and optical absorption) . More details of the laser model can be found elsewhere.^{10,14,15}

The drift-diffusion model with Fermi statistics is used for the 2D carrier transport. Thermionic emission theory is used at heterojunctions where the carrier transport is mainly related to the band offset ($\Delta E_c / \Delta E_g$) for which a typical value of 0.4 is assumed.¹⁴ The QWs are assumed to have a step-wise potential profile with parabolic sub-bands. Phonon-assisted scattering between confined and unconfined quantum states is not considered explicitly. More sophisticated models are needed to study the laser dynamics.¹⁶ The effective index method is used for the optical mode calculation. We assume that the transistor laser is to be operated in the normal transistor-behavior region without considering collector breakdown. Therefore impact ionization and Zener tunneling are not included. Thermal effect is not considered.

Several main sources of carrier recombination are considered. Stimulated emission and spontaneous emission in the QWs are calculated from the band structure and Fermi distribution. The spontaneous emission parameter is assumed to be $B = 10^{-10} \text{ cm}^3 \cdot \text{s}$ within the passive layers.¹⁴ The SRH recombination lifetimes of electrons and holes are assumed to be 20 ns in the QWs and 100 ns in the other layers.¹⁴ Although InGaAsP/InP has less surface recombination than GaAs,¹⁷ it cannot be ignored for the deeply etched structure and may be critical for a small ($\sim 1 \mu\text{m}$ width) waveguide.¹⁸ The surface recombination velocity is assumed to be $2.5 \times 10^4 \text{ cm/s}$. The value can be reduced to below $4 \times 10^3 \text{ cm/s}$ by surface passivation.¹⁸ The Auger recombination is calculated by¹⁹

$$R_{aug} = (C_n n + C_p p) \times (np - n_i^2) \quad (1)$$

where n and p are electron and hole densities, respectively. The Auger coefficients $C_p = 1.6 \times 10^{-28} \text{ cm}^6 \cdot \text{s}^{-1}$ and $C_n = 0$ are used¹⁴ by assuming that the CHHS Auger process dominates.²⁰

Also important to the transistor laser is the optical absorption due to the existence of the heavily doped layer close to the active region. A small background loss of $\alpha_b = 5 \text{ cm}^{-1}$ is assumed for the carrier-density-independent mechanisms like defect scattering. The free-carrier absorption due to electrons can be neglected since the heavily doped n-type layer are far away from the peak of the optical mode and the absorption coefficient is very small in InGaAsP/InP lasers ($k_n = 10^{-18} \text{ cm}^2$).¹⁴ Absorption within the valence bands due to intraband (i.e., free carrier absorption) or interband transitions is the dominant absorption mechanism in InGaAsP/InP lasers which is roughly proportional to the hole density. The hole absorption coefficient $k_p = 3.7 \times 10^{-17} \text{ cm}^2$ is assumed.²¹

To evaluate the physical models and parameters, a conventional ridge-waveguide laser diode is simulated and compared with the experiment. It's epitaxial structure is shown in Table 2. It has the same MQW system (the central wavelength of the photoluminescence is at 1548 nm at room temperature) and same waveguide material as the proposed transistor laser in Table 1. The light output and current vs. voltage (LIV) curves of the simulation have been matched to the experiment as shown in Figure 1.

4. RESULTS AND DISCUSSION

In the previous section, the laser simulation tool and parameters have been validated using a conventional laser. Next, our designed transistor laser is modeled. The transistor laser is operated in the common-emitter configuration, as shown in Figure 2, with the emitter-base junction forward biased and the base-collector junction reverse biased.

The collector IV curves for different base current I_B are shown in Figure 3, illustrating the typical transistor characteristics with an electrical gain β around $2 \sim 4$. The optical output power from the front facet as a function of the base current I_B is shown in Figure 4. There are three regions in each LI curve: below laser threshold, lasing linear region, and lasing saturation region. The threshold is $\sim 7 \text{ mA}$ which is comparable with the laser diode that is tested in Section 3. The low threshold is expected due to the good optical confinement (as shown in Figure 2) and reduced lateral leakage current. The slope efficiency of the linear region is 25.3% which is a little lower than the fabricated conventional laser diode ($\sim 29.4\%$) due to the higher optical absorption and large surface recombination. This can be improved by surface passivation.¹⁸

Table 2. The epitaxial structure of the conventional 1550 nm ridge-waveguide laser diode.

Layer	Composition	Thickness (nm)	Doping ($10^{18}/cm^3$)
Contact	$In_{0.53}Ga_{0.47}As$	200	p+, Zn, 20
Cladding	InP	1600	n, Si, 0.7 ~ 1.0
Etching-stop	$In_{0.89}Ga_{0.11}As_{0.24}P_{0.76}$	10	n, Si, 0.7
Waveguide	$In_{0.76}Ga_{0.24}As_{0.53}P_{0.47}$	100	Undoped
6 Wells / 5 Barriers	$In_{0.81}Ga_{0.19}As_{0.76}P_{0.24}$ / $In_{0.76}Ga_{0.24}As_{0.53}P_{0.47}$	6 / 9	Undoped
Waveguide	$In_{0.76}Ga_{0.24}As_{0.53}P_{0.47}$	100	Undoped
Buffer	InP	1200	n, Si, 1.0
Substrate	InP	-	n, Si, 3.0

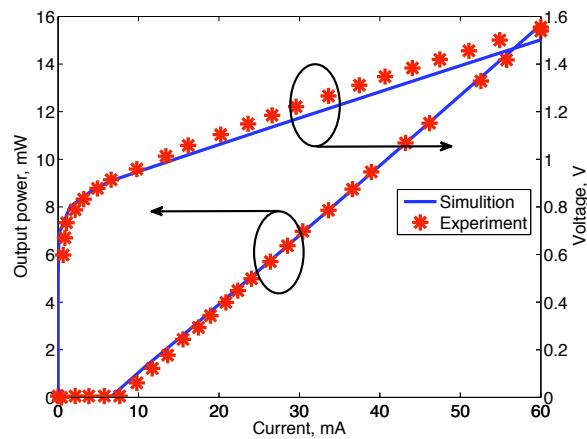


Figure 1. Simulated and experimental LIV curves of a ridge-waveguide laser diodes. The ridge waveguide is $2 \mu m$ wide, $1.8 \mu m$ high, and $250 \mu m$ long. The front and back reflectivities are 90% and 30%, respectively. The laser was mounted on a thermal sink and tested at $25^\circ C$.

As shown in the Figure 4, the saturation power depends on the emitter-collector voltage V_{CE} which determines the bias condition of the base-collector junction at a certain base voltage V_B (V_B increases as I_B increases). When V_B is so high that the base-collector junction is partially turned on, the collector current is reduced and the optical power goes to saturation because the extra injected holes from the base go to the collector instead of the active region for additional stimulated emission. The typical electron current distributions at different bias conditions are shown in Figure. 5. We can see that while in the linear region, almost all the electrons flow from the emitter to the active region and are then collected by the collector (note that the current direction is opposite to the electron flow), in the saturation region some electrons escape from the collector to the base. This optical saturation of the transistor laser has been investigated in the numerical modeling of a transistor VCSEL and attributed to the three-port operation based on which a voltage-controlled laser operation was proposed.⁴ Here we have found that this effect is present in both VCSELs as well as edge emitting lasers. The optical power vs. V_{CE} (LV) curves of the transistor laser is shown in Figure 6. Similar to the LI curve, the LV curve also has three regions. The voltage threshold is $\sim 1V$. The saturation power in the LV curve in this case depends on the base current.

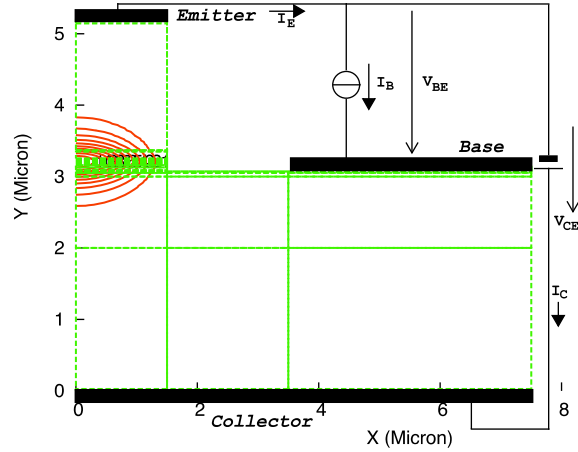


Figure 2. The bias configuration and optical mode of the transistor laser. The structure is symmetric in the x-axis mirrored at $x = 0$. Only half is shown. The center of the contours are in the QWs, indicating a strong overlap between the optical mode and the active gain region.

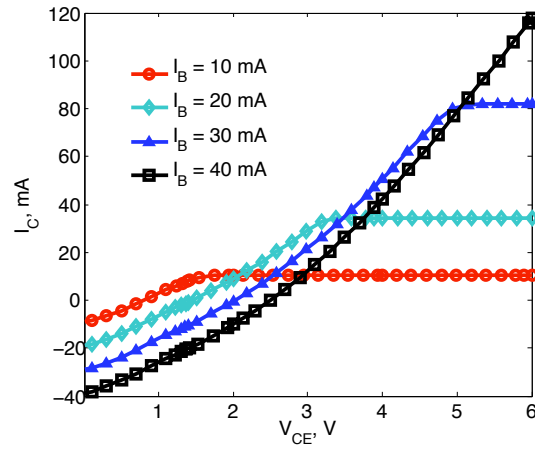


Figure 3. Simulated current-voltage ($I_C - V_{CE}$) characteristics of the transistor lasers.

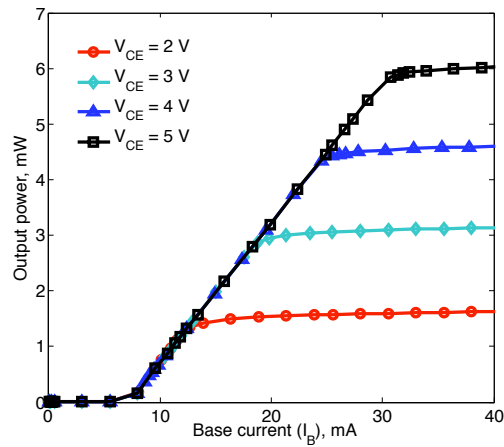


Figure 4. Simulated LI curves of the transistor laser for the different collector-emitter voltages.

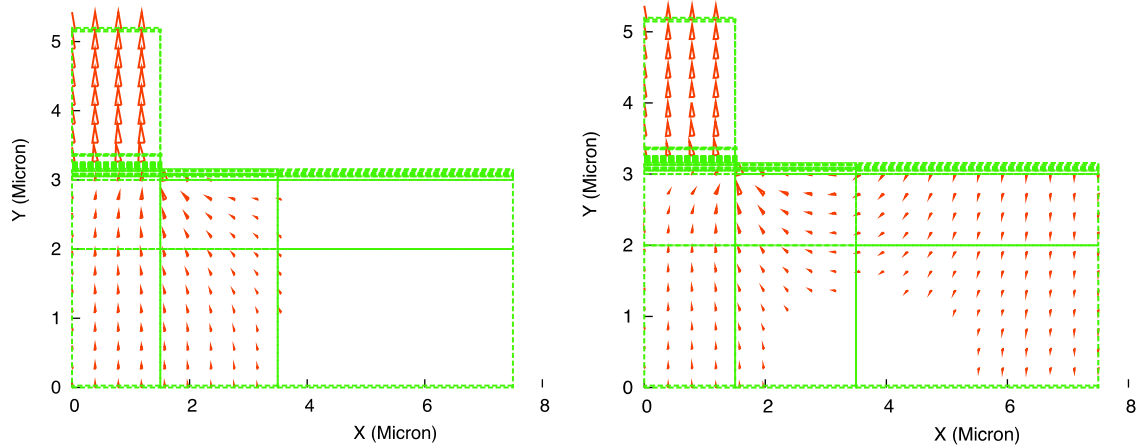


Figure 5. Cross-section view of the electron current distribution in the transistor laser at $I_B = 10\text{mA}$ (left, where base-collector junction is reverse biased) and $I_B = 60\text{mA}$ (right, where base-collector junction is forward biased and partially turn-on) with $V_{CE} = 3\text{V}$. The structure is symmetric in the x-axis mirrored at $x = 0$. Only half is shown.

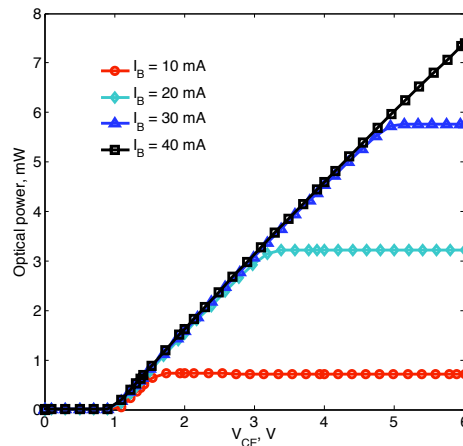


Figure 6. Simulated optical output power as a functions of the emitter-collector voltage V_{CE} for the different base currents.

5. CONCLUSION

While the transistor laser has many interesting features, the big question is whether we can design a transistor laser with good laser performance, i.e. low threshold and high slope efficiency. In this paper we have numerically modeled an InGaAsP-InP MQW transistor laser at 1550 nm. The key features of the device are the deep ridge structure (i.e., the QWs are etched through) and an asymmetric doping profile in the base. The purpose of this design is to reduce the carrier recombination outside the QWs and reduce the optical loss. Our numerical modeling shows a < 10 mA threshold and a $> 25\%$ slope efficiency. Having verified our model by match the simulation to a fabricated conventional laser, this work demonstrates a good transistor-laser design and bring the transistor laser closer to practical applications.

ACKNOWLEDGMENTS

The UBC authors acknowledge the support of the British Columbia Innovation Council (BCIC), the Natural Sciences and Engineering Research Council of Canada (NSERC), and Crosslight Software Inc. Z. Duan acknowledges the support of the Ministry of Science and Technology (MOST) of China (the International Cooperation Project, Grant No. 2008DFA11010).

REFERENCES

- [1] Holonyak, N. and Feng, M., "The transistor laser," *IEEE Spectrum*. **43**, 50–55 (2006).
- [2] Faraji, B., Shi, W., Pulfrey, D. L., and Chrostowski, L., "Analytical modeling of the transistor laser," *IEEE J. Quantum Electron.* **15**, 594–603 (2009).
- [3] Faraji, B., Shi, W., Pulfrey, D. L., and Chrostowski, L., "Common-emitter and common-base small-signal operation of the transistor laser," *Applied Physics Letters* **93**, 143503 (2008).
- [4] Shi, W., Chrostowski, L., and Faraji, B., "Numerical study of the optical saturation and voltage control of a transistor vertical cavity surface emitting laser," *IEEE Photonics Technology Letters*. **20**, 2141–2143 (2008).
- [5] Feng, M., N. Holonyak, J., Then, H. W., We, C. H., and Walter, G., "Tunnel junction transistor laser," *Applied Physics Letters* **94**, 041118 (2009).
- [6] Dixon, F., Feng, M., N. Holonyak, J., Huang, Y., Zhang, X. B., Ryou, J. H., and Dupuis, R. D., "Transistor laser with emission wavelength at 1544 nm," *Applied Physics Letters* **93**, 021111 (2008).
- [7] Feng, M., Holonyak, N., Then, H. W., and Walter, G., "Charge control analysis of transistor laser operation," *Applied Physics Letters* **91**, 053501 (2007).
- [8] Faraji, B., Pulfrey, D. L., and Chrostowski, L., "Small-signal modeling of the transistor laser including the quantum capture and escape lifetimes," *Applied Physics Letters* **93**, 103509 (2008).
- [9] Feng, M., N. Holonyak, J., Walter, G., and Chan, R., "Room temperature continuous wave operation of a heterojunction bipolar transistor laser," *Applied Physics Letters* **87**, 131103 (2005).
- [10] [*Crosslight Device Simulation Software – A General Description*], Crosslight Software Inc. (2005).
- [11] Huang, Y., Zhang, X.-B., Ryou, J.-H., Dupuis, R. D., Dixon, F., Holonyak, N., and Feng, M., "AlGaAs/InP light-emitting transistors operating near 1.55 μm ," *J. Appl. Phys.* **103**, 114505 (2008).
- [12] Katz, A., Thomas, P. M., Chu, S. N. G., Dautremont-Smith, W. C., Sobers, R. G., , and Napholtz, S. G., "Pt/Ti Ohmic contact to p⁺⁺-ingaasp (1.3 μm) formed by rapid thermal processing," *J. Appl. Phys.* **67**, 884–889 (1990).
- [13] Jian, P., Ivey, D. G., Bruce, R., and Knight, G., "Microstructural study of Au-Pd-Zn ohmic contacts to p-type ingaasp-inp," *Journal of materials sciences: materials in electronics* **7**, 77–83 (1996).
- [14] Piprek, J., Abraham, P., and Bowers, J. E., "Self-consistent analysis of high-temperature effects on strained-layer multiplequantum-well InGaAsP-InP lasers," *IEEE J. Quantum Electron.* **36**, 366–374 (2000).
- [15] Li, Z.-M., "Physical models and numerical simulation of modern semiconductor lasers," *Proc. SPIE* **2994**, 698–708 (1997).
- [16] Grupen, M. and Hess, K., "Simulation of carrier transport and nonlinearities in quantum-well laser diodes," *IEEE J. Quantum Electron.* **34**, 120–140 (1998).
- [17] Coldren, L. A. and Corzine, S. W., [*Diode lasers and photonic integrated circuits*], John Wiley & Sons, Inc., New York (1995).
- [18] Amarnath, K., Grover, R., Kanakaraju, S., and Ho, P.-T., "Electrically pumped InGaAsP-InP microring optical amplifiers and lasers with surface passivation," *IEEE Photon. Technol. Lett.* **17**, 2280–2282 (2005).
- [19] Liou, B.-T., Y, S.-H., Yao, M.-W., Chen, M.-L., Y, K. K., and Chang, S.-H., "Numerical study for 1.55 μm AlGaInAs/InP semiconductor lasers," *Proc. SPIE* **6368**, 636814 (2006).
- [20] Seki, S., Lui, W. W., and Yokoyama, K., "Explanation for the temperature insensitivity fo the Auger recombination rates in 1.55 μm inp-based strained-layer quantum-well lasers," *Appl. Phys. Lett.* **66**, 3093–3095 (1995).
- [21] Joindot, I. and Beylat, J. L., "Intervalence band absorption coefficient measurements in bulk layer, strained and unstrained multiquantum well 1.55 μm semiconductor lasers," *Electron. Lett.* **29**, 604–606 (1993).